Journal of King Saud University – Science (2017) 29, 311–319

King Saud University
Journal of King Saud University – Science
www.ksu.edu.sa
www.sciencedirect.com

Computational study and in vitro evaluation of the anti-proliferative activity of novel naproxen derivatives

Abdullah G. Al-Sehemi [a,b], Ahmad Irfan [a,b,*], Mohammad Alfaifi [c], Ahmed M. Fouda [a], Tarek Ma'mon El-Gogary [d], Diaa A. Ibrahim [d]

[a] *Department of Chemistry, Faculty of Science, King Khalid University, Abha 61413, P.O. Box 9004, Saudi Arabia*
[b] *Research Center for Advanced Materials Science (RCAMS), King Khalid University, Abha 61413, P.O. Box 9004, Saudi Arabia*
[c] *Department of Biology, Faculty of Science, King Khalid University, Abha 61413, P.O. Box 9004, Saudi Arabia*
[d] *Faculty of Science, Jazan University, Jazan, Saudi Arabia*

Received 7 September 2016; revised 24 December 2016; accepted 5 January 2017
Available online 18 January 2017

KEYWORDS

Biological active compounds;
Naproxen derivatives;
Quantitative structure–activity relationship;
Electro-optical properties;
Antiproliferative activity

Abstract In the present work, five naproxen derivatives, i.e., 3-amino-(4E)-5-imino-1-[2-(6-methoxy-2-naphthyl)propanoyl]-4-(benzylidene)-4,5-dihydro-1*H*-pyrazole (**a**), 3-amino-(4E)-5-imino-1-[2-(6-methoxy-2-naphthyl)propanoyl]-4-(4-bromobenzylidene)-4,5-dihydro-1*H*-pyrazole (**b**), 3-amino-(4E)-5-imino-1-[2-(6-methoxy-2-naphthyl)-propanoyl]-4-(4-methoxybenzylidene)-4,5-dihydro-1*H*-pyrazole (**c**), 3-amino-(4E)-5-imino-1-[2-(6-methoxy-2-naphthyl)propanoyl]-4-(4-methylbenzylidene)-4,5-dihydro-1*H*-pyrazole (**d**), 3-amino-(4E)-5-imino-1-[2-(6-methoxy-2-naphthyl)propanoyl]-4-(4-nitrobenzylidene)-4,5-dihydro-1*H*-pyrazole (**e**) were synthesized then characterized by FTIR, ^{1}H and ^{13}C NMR techniques. The ground state geometries were optimized by B3LYP functional of density functional theory (DFT) with three different basis sets (6-31G*, 6-31G** and 6-31 + G**). The absorption wavelengths, oscillator strengths and major transitions were calculated using time dependent DFT. The effect of electron withdrawing groups ($–NO_2$ and –Br) and electron donating groups ($–CH_3$ and $–OCH_3$) was intensively studied with respect to structure–activity relationship (SAR), quantitative structure–activity relationship (QSAR), frontier molecular orbitals (FMOs), molecular electrostatic potentials (MEP) and global reactivity descriptors. By the analysis of molecular docking work, it was found that pure hydrophobic substitution at position 4 of aldehyde part is more favorable than hydrophilic one. Compound **c** showed strong anti-proliferative

* Corresponding author at: Department of Chemistry, Faculty of Science, King Khalid University, Abha 61413, P.O. Box 9004, Saudi Arabia. Fax: +966 172418426.
E-mail address: irfaahmad@gmail.com (A. Irfan).
Peer review under responsibility of King Saud University.

Production and hosting by Elsevier

http://dx.doi.org/10.1016/j.jksus.2017.01.003

activity against MCF-7 cells with IC_{50} value of 1.49 μM, and compound **d** showed moderate activity. The docking studies revealed that normal alkane chain is improving the biological activity in compound **c**, which endorsed to bury well in the active site resulting to enhance the hydrophobic interactions. The newly synthesized compounds against tested cell lines showed stronger antiproliferative activity as compared to the naproxen.

1. Introduction

It is well-known that the continuous use of non-steroidal anti-inflammatory drugs (NSAIDs) cause bleeding, nephrotoxicity and gastro-intestinal ulcer (Nakka et al., 2010). Thus to reduce the side effects and to enhance the anti-inflammatory activity (AIA), derivatization of the carboxylate group is an important step (Duflos et al., 2001). Naproxen is being used as NSAID since long but due to its carboxylic acid group, there are some side effects. Previous studies showed that AIA can be boosted by incorporation or introduction of Pyrazole moiety (Youssef et al., 2010). It was shown previously that persistent inflammation can cause tumors. Moreover, the role of the epidermal growth factor receptor (EGFR) system in inflammation-related cell signaling was investigated (Carmen, 2009). The EGFR was intricate in epithelial growth as well (Hamilton et al., 2003). Moreover, the naproxen exhibited proficient anti-proliferative action (Kim et al., 2014; Lubet et al., 2015). Based on the reported anti-proliferative activity of a great number of pyrazoles and naproxen moieties and in continuation of our research to syntheses of bioactive naproxen derivatives (Viale et al., 2013), we report herein the syntheses of N-naproxenylpyrazole derivatives to study their structural, electro-optical properties and anti-prolifrerative activity.

In the present work, we have synthesized five derivatives of naproxen, i.e., 3-amino-(4E)-5-imino-1-[2-(6-methoxy-2-naphthyl)propanoyl]-4-(benzylidene)-4,5-dihydro-1*H*-pyrazole (**a**), 3-amino-(4E)-5-imino-1-[2-(6-methoxy-2-naphthyl)propanoyl]-4-(4-bromobenzylidene)-4,5-dihydro-1*H*-pyrazole (**b**), 3-amino-(4E)-5-imino-1-[2-(6-methoxy-2-naphthyl)propanoyl]-4-(4-methoxybenzylidene)-4,5-dihydro-1*H*-pyrazole (**c**), 3-amino-(4E)-5-imino-1-[2-(6-methoxy-2-naphthyl)propanoyl]-4-(4-methyl benzylidene)-4,5-dihydro-1*H*-pyrazole (**d**), 3-amino-(4E)-5-imino-1-[2-(6-methoxy-2-naphthyl)propanoyl]-4-(4-nitrobenzylidene)-4,5-dihydro-1*H*-pyrazole (**e**), see Scheme 1 then characterized by FTIR, ^{1}H and ^{13}C NMR techniques. In these derivatives benzene and pyrazole moieties (Youssef et al., 2010) were introduced with the aim to minimize the side effects and to increase the drug like properties. The effect of electron withdrawing groups (EWDGs), i.e.; NO_2 and Br and electron donating groups (EDGs), i.e.; CH_3 and OCH_3 has been studied on the properties of interests, like, frontier molecular orbitals (FMOs), (highest occupied molecular orbitals (HOMOs), lowest unoccupied molecular orbitals (LUMOs), energy gaps (E_{gap}), absorption wavelengths, molecular electrostatic potentials (MEP), and global reactivity descriptors (hardness, softness, electronegativity, chemical potential and electrophilicity indices). In this study, the crystal structure of EGFR tyrosine kinase in DFG-out conformation (PDB code 4HJO) was selected to perform molecular docking for EGFR inhibitors as well. Moreover, the structure–activity relationship (SAR), quantitative structure–activity relationship (QSAR), docking score, binding energies, cytotoxicity and anti-prolifrerative activity has been studied and discussed.

2. Methodology

2.1. Experimental methodology

Melting points of chemicals purchased from Sigma–Aldrich were determined with a Stuart Scientific Co. Ltd apparatus and are uncorrected. The Jasco FT/IR 460 plus spectrophotometer was used to determine the IR spectra. BRUKER AV 500/600 MHz spectrometer was used to record the ^{1}H NMR and ^{13}C NMR spectra.

Compound (III) prepared as previously described (Nakka et al., 2010)

The reaction of 2-(6-methoxy-naphalen-2-yl)-propionic acid hydrazide with arylidenemalononitrile (IVa-e)

A mixture of the arylidenemalononitrile (IVa-e) (0.001 mol) and 2-(6-methoxy-naphalen-2-yl)-propionic acid hydrazide (0.001 mol) in ethanol (30 ml) was heated under reflux for 4 h (monitored with TLC). The solvent was evaporated in *vacuo* and obtained residue was poured onto water and stirred at r.t for 20 min. The obtained solid was filtered off, dried and recrystallized from ethanol to afford (Va-e).

The physical and spectral data of compounds Va-e are as follows:

3-amino-(4E)-5-imino-1-[2-(6-methoxy-2-naphthyl)propanoyl]-4-(benzylidene)-4,5-dihydro-1*H*-pyrazole (**a**).

Yield 80%, m.p 188–190 °C, ^{1}H NMR (DMSO-d6) δ 8.22 (s, 1H, NH), δ 7.17.-7.92 (11 ArH), δ 7.13 (1H, CH = C), δ 4.8 (2H, NH_2) δ 3.87(3H, OCH_3), δ 3.35(q, 1H), δ 1.51 (3H, CH_3); ^{13}C NMR (125 MHz, DMSO-d6) δ 174.9, 169.8, 156.9, 146.6, 137.1, 136.6, 133.2, 133, 129.9, 129.1, 128.9, 128.7, 128.3, 126.7,; 126.2, 125.6, 118.6, 118.5, 105.6, 55.1, 43.9, 18.4, IR (KBr, υmax cm -1) 3187 (NH), 1653 (CO), 1605 (C = N).

3-amino-(4E)-5-imino-1-[2-(6-methoxy-2-naphthyl)propanoyl]-4-(4-bromobenzylidene)-4,5-dihydro-1*H*-pyrazole (**b**).

Yield 82%, m.p 206–208 °C, ^{1}H NMR (DMSO-d6) δ 8.19 (s, 1H, NH), δ 7.16–7.91 (10 ArH), δ 7.02 (1H, CH = C), δ 4.8 (2H, NH_2), δ 3.92 (q, 1H), δ 3.83(3H, OCH_3), δ 1.53 (3H, CH_3); ^{13}C NMR (125 MHz, DMSO-d_6) *δ*; 174.7, 169.6, 160.7, 157, 146.5, 137.2, 136.8, 133.2, 133, 129.1, 129, 128.5, 128.4, 128.2, 126.3, 125.9, 118.6, 114.30, 105.7, 55.17, 43.9, 18.5; IR (KBr, υ_{max} cm^{-1}) 3179 (NH), 1650 (CO), 1606 (C = N).

3-amino-(4E)-5-imino-1-[2-(6-methoxy-2-naphthyl)propanoyl]-4-(4-methoxybenzylidene)-4,5-dihydro-1*H*-pyrazole (**c**).

Yield 84%, m.p 205–207 °C, ^{1}H NMR (DMS00O-d6) δ 8.16 (s, 1H, NH), δ 7.11–7.86 (10 ArH), δ 6.99 (1H,

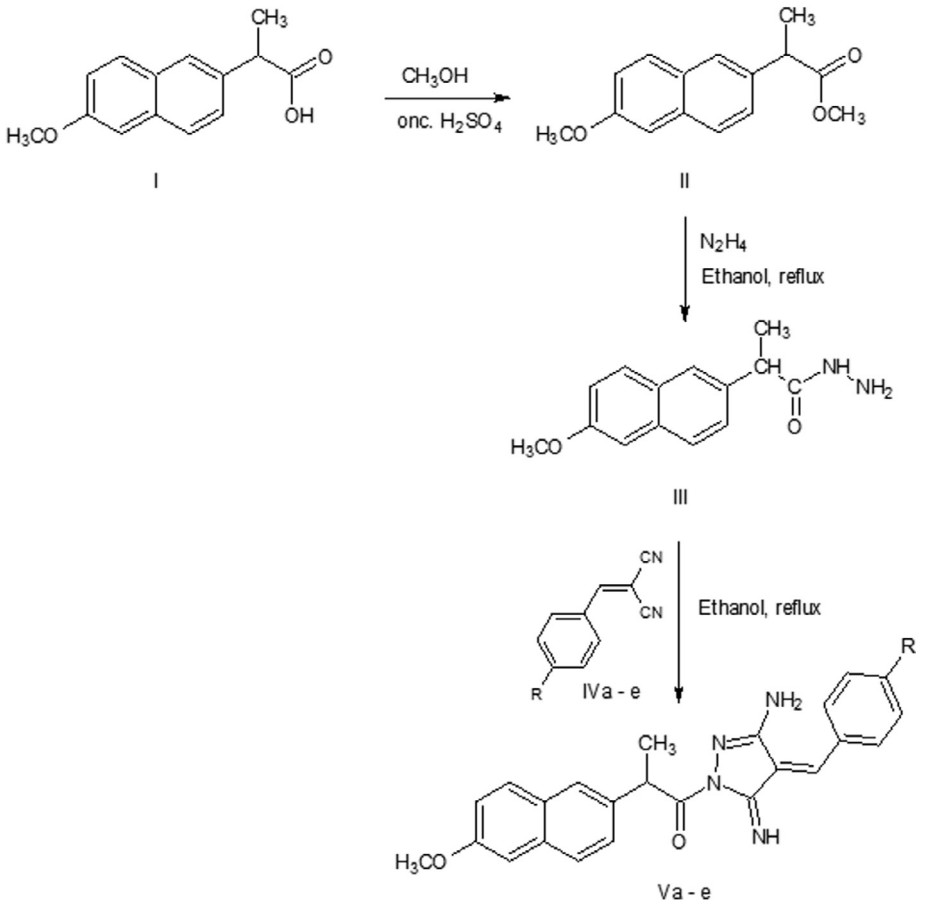

Scheme 1 The synthetic scheme of naproxen derivatives (R = H for a, 4-Br for b, 4-OCH_3 for c, 4-CH_3 for d, 4-NO_2 for e).

CH = C), δ 4.78 (2H, NH_2), δ 3.86 (q, 1H), δ 3.78(6H, 2, -OCH_3), δ 1.50 (3H, CH_3); ^{13}C NMR (125 MHz, DMSO-d_6) *δ*; 174.7, 169.5, 160.7,156.9, 146.5, 137.2, 133.2, 133, 129, 128.5, 128.4, 128.2, 126.8, 126.7, 126.2, 125.6, 118.6, 114.2, 105.7, 55.2, 43.9, 18.4; IR (KBr, υ_{max} cm^{-1}) 3179 (NH), 1650 (CO), 1606 (C = N).

3-amino-(4E)-5-imino-1-[2-(6-methoxy-2-naphthyl)propanoyl]-4-(4-methylbenzylidene)-4,5-dihydro-1*H*-pyrazole (**d**).

Yield 80%, m.p 193–195 °C, ^{1}H NMR (DMSO-d6) δ 8.21 (s, 1H, NH), δ 7.17.-7.92 (10 ArH), δ 7.15 (1H, CH = C), δ 4.82(2H, NH_2) δ 3.9(3H, OCH_3), δ 3.39(q, 1H), δ 1.53 (3H, CH_3); ^{13}C NMR (125 MHz, DMSO-d_6) *δ* 174.9, 169.7, 157.1, 146.6, 139.4, 137.1, 133, 131.5, 129.4, 129, 128.4, 126.9, 126.8, 126.3, 125.7, 125.4, 118.6, 105.7, 55.1, 43.9, 20.9, 18.4; IR (KBr, υ_{max} cm^{-1}) 3184 (NH), 1659 (CO), 1606 (C = N).

3-amino-(4E)-5-imino-1-[2-(6-methoxy-2-naphthyl)propanoyl]-4-(4-nitrobenzylidene)-4,5-dihydro-1*H*-pyrazole (**e**).

Yield 81%, m.p 216–218 °C, ^{1}H NMR (DMSO-d6) δ 8.28 (s, 1H, NH), δ 7.13.-7.95 (10 ArH), δ 7.11 (1H, CH = C), δ 4.81(2H, NH_2) δ 3.87(3H, OCH_3), δ 3.35(q, 1H), δ 1.52 (3H, CH_3); ^{13}C NMR (125 MHz, DMSO-d6) δ 170.2, 157.1, 157, 147.7, 144.1, 140.6, 136.8, 133.27, 133, 129.1, 129, 128.4, 127.5, 126.7, 126.2, 125.4, 123.9, 118.6, 105.6, 55.1, 44, 18.4;; IR (KBr, υmax cm -1) 3179 (NH), 1660 (CO), 1604 (C = N).

2.2. Computational Details

Quantum chemical methods (Li et al., 2012; Chaudhry et al., 2014; Irfan et al., 2014; Zgierski et al., 2014; Irfan et al., 2015, 2016) particularly density functional theory (DFT) and time dependent DFT (TDDFT) Salvatori et al., 2014; Fu et al., 2014 gained significant attention to reproduce the experimental data as well as to predict the different properties of interests. Previously, it has been proved that among different DFT methods (Sadasivam et al., 2012; Chen et al., 2014; Irfan and Al-Sehemi, 2014; Irfan et al., 2015a,b,c, 2014), B3LYP functional is sound and reasonable approach to reproduce the experimental evidences (Irfan et al., 2014; Irfan, 2014a,b). Sousa et al. examined the geometrical parameters and photochemical properties of anti-inflammatory drugs and observed that B3LYP is the superlative functional than the B1B95, B97-2, BP86 and BPW91 ones (Musa and Eriksson, 2008). Here, the optimized ground state geometries were obtained at B3LYP/6-31G* level of theory. No imaginary frequency was observed after the frequency calculations. Further, the optimized coordinates were taken and geometry optimizations were performed at higher levels of theories at B3LYP/6-31G** and B3LYP/6-31+G** (Petersson and Al-Laham, 1991; Miehlich et al., 1989; Becke, 1993; Kohn et al., 1996). The global reactivity descriptors were calculated at B3LYP/6-31+G** levels of theory. Details about methodology

can be found in the reference (Al-Sehemi et al., 2016) and supporting information.

To understand the radical scavenging behavior of naproxen derivatives (**a-e**), we have studied the one-electron transfer mechanism (Belcastro et al., 2006; Wright et al., 2001). Then absorption wavelengths were calculated by adopting the TDDFT. All above mentioned calculations were performed by Gaussian09 package (M. J. Frisch et al., 2009). In the next step, the optimized coordinates were imported to Spartan '14 v1.1.8' software and QSAR studies were executed at B3LYP/6-31G** level of theory.

Discovery Studio (DS 2.0) package was used to prepare the Protein Structure. The structures were aligned after adding the invalid or missing residues using the protein structure alignment module. The structures were minimized after adding the hydrogen atoms by adopting the CHARMM force field (Soteras Gutiérrez et al., 2016; Vanommeslaeghe and MacKerell, 1850). The compounds were optimized by DFT (B3LYB method) in docking calculations. Docking study was validated by re-docking the native ligand; erlotinib, which gave docking pose with RMSD value of 1.23 Å.

3. Results and discussion

3.1. Electro-optical properties

In Fig. 1, the distribution patterns of the FMOs (HOMOs and LUMOs) at the ground states have been illustrated. The HOMO and LUMO in naproxen is distributed on the main core. In all the naproxen derivatives studied here, the HOMOs are delocalized at naphthalene moiety while LUMO are distributed on the benzylidene-4H-pyrazole moieties. The comprehensive intra-molecular charge transfer (ICT) was observed from HOMOs to LUMOs in all the studied systems. The maximum ICT was perceived in e where strong EWDGs is attached that attracts the electronic density toward itself. In Table S1, computed HOMO energies (E_{HOMO}), LUMO energies (E_{LUMO}), HOMO–LUMO energy gaps (E_g) and global reactivity descriptors of compounds **a-e** obtained at B3LYP/6-31 + G** levels of theory have been tabulated. The E_{HOMO} and E_{LUMO} of compound **a** were observed −5.60 and −2.74 eV, respectively. The E_{HOMO} level rises by substituting the EWDG –Br and $–NO_2$ at para position, i.e., 0.05 and 0.17 eV as compared to compound **a**. The introduction of EDG $–CH_3$ increases while $–OCH_3$ declines E_{HOMO} level at the same position 0.08 and 0.05 eV, respectively. The E_{LUMO} level rises by substituting the EWDGs at para position, i.e., 0.17 and 0.90 eV as compared to compound **a**. The introduction of EDGs $–CH_3$ and $–OCH_3$ lower the E_{LUMO} level 0.15 eV. The significant variation in the E_{HOMO} and E_{LUMO} level was noticed in compound **e** in which strong EWDG was at para position. Substituting the EWDG would lead to reduce the E_g while EDGs increases it.

In compound **a**, two major absorption peaks have been observed, i.e., maximum λ_a peak at 304 nm and second peak at 449 nm. By substituting the EDG $–OCH_3$ (compound **c**) maximum λ_a peak shifted at 329 nm (red shifted 25 nm compared to compound **a**) while second peak at 440 nm (blue shifted 9 nm compared to parent molecule). The introduction of EDG $–CH_3$ at para position (compound **d**) would lead to 9 nm red shift maximum λ_a peak at 315 nm while 25 nm blue shifted in the second peak, i.e., 424 nm compared to compound **a**. By replacing –H of para position by EWDG –Br (compound **b**) and NO_2 (compound **e**) showed the maximum λ_a peaks at 320 and 527 nm which are being red shifted 16 and 223 nm compared to compound **a**. In compounds **b** and **e**, a second peak has been observed at 458 and 327 n, i.e., red and blue shifted 11 and 122 nm than that of compound **a**. It can be found from Fig. 2 that both the EDGs as well as EWDGs are leading the absorption toward longer wavelength (red shift). The largest red shift has been observed in compound **e** that contains the strong EWDG but it decreases

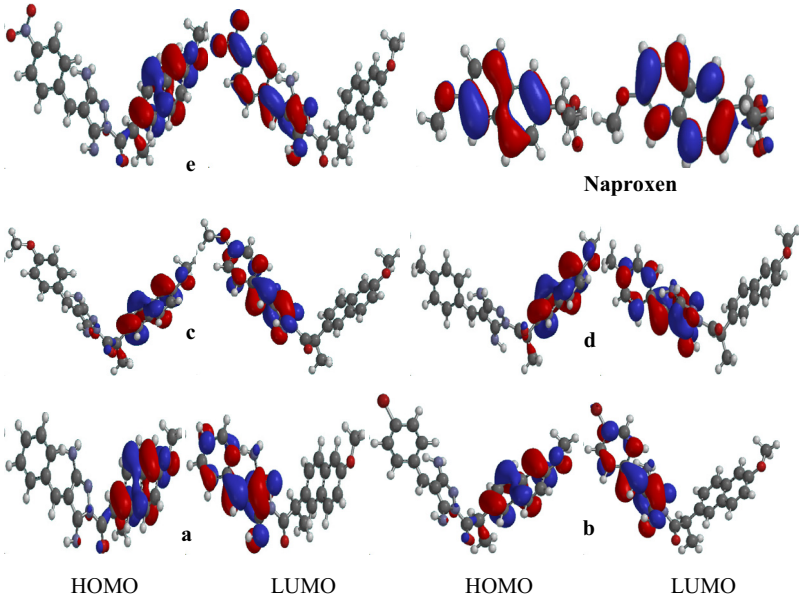

Fig. 1 The distribution pattern of the frontier molecular orbitals of naproxen derivatives a-e.

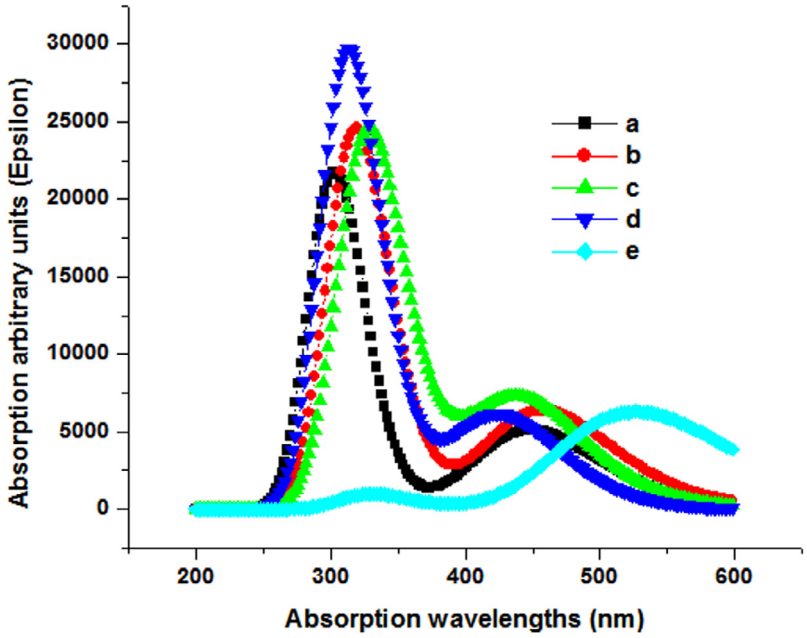

Fig. 2 Absorption spectra of naproxen derivatives a-e by TDDFT.

the oscillator strength value three to four times as compared to other studied compounds **a-d**.

3.2. Single electron transfer mechanism

The scavenging of free radicals can be understood by single electron endowment. The ionization potential (IP) is a vital physical factor to evaluate the range of electron transfer. By removing the electron from the HOMO, radical can be gained in one-electron transfer mechanism. The values of the ionization potential have been tabulated in Table S1. The trend in IP has been observed as **c** < **a** < **b** < **d** < **e** illuminating that in compound **e** electron transfer mechanism would be more promising for the scavenging of free radicals than those of the other naproxen derivatives. Compound **e** containing EDG $-OCH_3$ might be superior antioxidant material as compared to the other counterparts. This study is in good agreement with the previous study that EDG would lead to enhance the antioxidant ability of the compounds (Al-Sehemi and Irfan, 2013).

3.3. Molecular electrostatic potential

The 3-D mapping of MEP is worthy to understand the relative reactivity sites for nucleophilic and electrophilic attack. In Fig. 3, the MEP surface maps of naproxen derivatives have been presented. The red, blue and green color electrostatic potential (ESP) sites denote the negative, positive and zero potentials. The negative ESP regions are accompanying the electrophilic reactivity while positive ones are concomitant to nucleophilic reactivity. The negative and positive sites would be promising for the electrophile and nucleophile attack, respectively. The MEP surface mapping analyses showed that pyrazol moiety might be favorable for the electrophile attack while naphthalene core for the nucleophile attack. In naproxen negative region is on carboxyl group which would be favorable for electrophile attack. Additionally, positive regions can be observed on the methyl and methoxy groups in compounds **c** and **d** while negative region on nitro group in compound **e** displaying electrophile and nucleophile attack, respectively.

3.4. QSAR study

The structure–activity relationship (SAR) and quantitative structure–activity relationship (QSAR) are decent tools to shed light on the biological activity of drugs. These tools are being used to discern the correlation between the biological activity and its physicochemical properties in a drug. We have tabulated the physicochemical and QSAR descriptors of naproxen derivatives in Table 1, i.e., μD = dipole moment, area, volume, partition coefficient (LogP), hydrogen bond donor (HBD), hydrogen bond acceptor (HBA), polar surface area (PSA), solvation energy and polarizability. Previously, Palm et al. found the sigmoidal curve relationship between the oral absorption of drug and PSA (Katrin, 1998). Hitherto, it has been found that the brain penetration decreases when PSA increases. Earlier studies displayed that orally active drug for better transport by transcellular route must not exceed PSA 120 A^2 (van de Waterbeemd et al., 1998; Kelder et al., 1999) and <100 A^2 for brain penetration (van de Waterbeemd et al., 1998). It is expected that naproxen derivatives **a-e** might be good orally active as well as worthy for brain penetration drugs due to PSA $<$ 100 A^2. From Table 1, it can be found that the theoretical study about pharmacokinetics and pharmacology for "absorption, distribution, metabolism, and excretion (ADME)" showed that compounds **a-e** do not break Lipinski's rule assembling them favorable drug contestants (Lipinski et al., 1997, 2001, 2004).

3.5. Docking studies

Erlotinib, an EGFR inhibitor, was considered as a reference compound to rationalize the EGFR inhibitory activity of target compounds. The docking results and binding energy calcu-

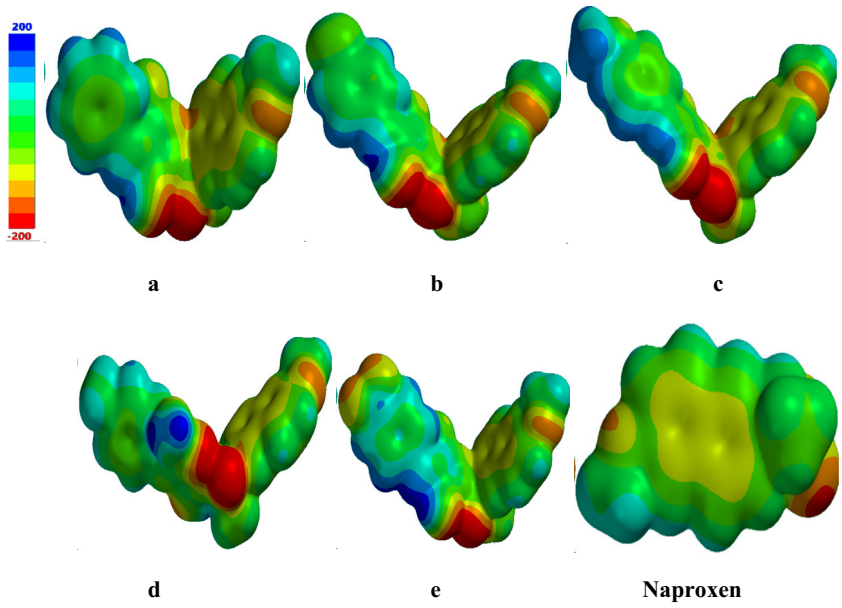

Fig. 3 The molecular electrostatic potential (MEP) surfaces of the naproxen derivatives.

Table 1 Different SAR descriptors of Naproxen and its derivatives obtained at B3LYP/6-31G** level of theory (μD = dipole moment; HBD = hydrogen bond donor; HBA = hydrogen bond acceptor; PSA = polar surface area; S.E. = solvation energy; Pol. = Polarizability).

	μD (Debye)	Area (A^2)	Volume (A^3)	Log P	HBD	HBA	Pol.	PSA (A^2)	S.E. (kJ/mol)
a	8.95	430.68	413.58	2.72	0	5	74.25	71.56	−70.42
b	7.08	450.78	431.66	3.33	0	4	75.74	71.64	−72.72
c	10.38	459.71	440.34	2.21	0	5	76.4	78.42	−77.37
d	5.96	449.27	431.77	3.12	0	5	75.66	71.77	−60.19
e	3.40	456.45	435.27	2.54	0	7	76.18	110.67	−77.5
Naproxen	1.37	261.24	242.01	1.32	1	2	59.91	41.448	−30.20

lations are shown in Table 2. Moreover, 2D interactions of native ligand; erlotinib into the active site of EGFR, 2D interactions of compounds with the active site and electrostatic interactions with EGFR binding pocket have been illustrated in Figs. S1–S7.

By the analyses of molecular docking work, we found that pure hydrophobic substitution at position 4 of aldehyde part is more favorable than hydrophilic substitution. Also, the normal chain alkane is enhancing the biological activity as found in compound **c**, which made it buried well in the active site as shown in Fig. S1 (enhance the hydrophobic interactions). All the modeling data are too close, which prove that hydrophobic interactions are more favorable than hydrogen bonds and electrostatic interactions. To clear the rational for biological activity of compound **c**, we carried out quantum docking of it with EGFR active site Fig. S1a. The results showed that compound **c** has the same interaction features as the native ligand (Erlotinib) and form the crucial hydrogen bond with MET769. The other hydrophobic interactions were the same as Erlotinib and this was proved by superimposing compound **c** over Erlotinib throughout quantum docking Fig. S1b. All these findings clear the reasons behind the activity of compound **c** over the other derivatives.

Table 2 Docking score and binding energy of studied compounds **a-e**.

Compounds	Docking Score	Binding Energy
a	−6.581	−53.497
b	−6.254	−57.159
c	−6.493	−56.860
d	−6.422	−55.693
e	−5.136	−54.324

3.6. In vitro cytotoxic screening

Cytotoxic activity of the new compounds, naproxen and doxorubicin was evaluated using Sulphorhodamine B (SRB) assay method (Skehan et al., 1990; Vichai and Kirtikara, 2006). Human colon cancer cells (HCT 116), Human hepatic carcinoma (HepG2) and Human breast cancer cells (MCF-7) were maintained in RPMI media supplemented with 100 μg/mL streptomycin, 100 units/ml penicillin and 10% heat-inactivated fetal bovine serum in a humidified, 5% (v/v) CO_2 atmosphere at 37 °C. Exponentially growing cells were detached from dishes using 0.25% trypsin-EDTA and plated in 96-well plates at 1000 cells/well. After 24 h of incubation,

Table 3 The IC_{50} (μM)[a] of tested compounds against human cancer cell lines.

Compounds	HCT116	HepG2	MCF-7
a	161.95	139.64	142.04
b	183.31	61.61	114.96
c	163.90	125.13	1.49
d	37.12	75.23	17.46
e	249.20	258.87	23.28
Naproxen	806.32	505.26	309.76
Doxorubicin	0.147	0.143	0.249

[a] IC_{50} is the compound concentration required to inhibit cell growth by 50%.

cells were exposed to various concentrations of tested compounds for 48 h. At the end of treatment time, cells were fixed with TCA (10%) for 1 h at 4 °C, washed several times with distilled water, stained with 0.4% SRB solution for 10 min in a dark place and washed with 1% glacial acetic acid. After drying overnight, Tris-HCl was used to dissolve the SRB-stained cells and the color intensity was measured at 570 nm using microplate reader (Anthos Zenyth-200RT, Cambridge, England). Doxorubicin was used as a positive control.

None of the tested compounds showed toxicity against HCT 116 and HepG2 cells (IC_{50} > 30.0 μM). On the other hand, compound **c** showed strong antiproliferative activity against MCF-7 cells with IC_{50} value of 1.49 μM, and compound **d** showed moderate activity while compound **e** showed weak activity against the same cell line with IC_{50} values of 17.64 and 23.28 μM respectively. Despite the weak and moderate antiproliferative activity of the newly synthesized compounds against tested cell lines, they showed stronger activity comparing to naproxen, see Table 3.

4. Conclusions

The comprehensible ICT was observed from HOMOs to the LUMOs of naproxen derivatives. The electron withdrawing groups (–Br and $–NO_2$) usually elevate while electron donating group ($–OCH_3$) decreases the HOMO and LUMO energy levels. The noteworthy variation in the HOMO and LUMO energy levels was viewed in compound **e** containing the strong EWDGs at para position resulting to reduce the energy gap. The introduction of EDGs and EWDGs at para positions would lead the maximum absorption spectral peaks toward red shift. The negative region (red color) on pyrazole moiety would encourage the electrophile attack while positive region (blue color) on naphthalene core might be promising for the nucleophile attack. The smaller PSA (< 100 A^2) of naproxen derivatives is deducing that these compounds might be good orally active and efficient brain penetration drugs. Compound **c** showed strong antiproliferative activity against MCF-7 cells with IC_{50} value of 1.49 μM, and compound **d** showed moderate activity. Compound **c** has the same interaction features as the native ligand (Erlotinib) and form the crucial hydrogen bond with MET769. Moreover, the normal alkane chain of compound **c** helps to buried well in active site which further boost the hydrophobic interactions. All the modeling data are too close, which prove that hydrophobic interactions are more favorable than hydrogen bonds and electrostatic interactions. Despite the weak and moderate antiproliferative activity of the newly synthesized compounds against tested cell lines, they showed stronger activity comparing to naproxen. Present computational investigations of the compounds' properties would help to design better drug contenders in the future.

Acknowledgement

We acknowledge the "Research Center for Advanced Materials Science (RCAMS), King Khalid University, Saudi Arabia" for providing the technical facilities to carry out this research work.

Appendix A. Supplementary data

Supplementary data associated with this article can be found, in the online version, at http://dx.doi.org/10.1016/j.jksus.2017.01.003.

References

Al-Sehemi, A.G., Irfan, A., 2013. Effect of donor and acceptor groups on radical scavenging activity of phenol by density functional theory. Arabian J. Chem. http://dx.doi.org/10.1016/j.arabjc.2013.06.019.

Al-Sehemi, A.G., Irfan, A., Aljubiri, S.M., Shaker, K.H., 2016. Density functional theory investigations of radical scavenging activity of 3′-Methyl-quercetin. J. Saudi. Chem. Soc. 20 (Supplement 1), S21–S28.

Becke, A.D., 1993. Density-functional thermochemistry. III. The role of exact exchange. J. Chem. Phys. 98, 5648–5652.

Belcastro, M., Marino, T., Russo, N., Toscano, M., 2006. Structural and electronic characterization of antioxidants from marine organisms. Theor. Chem. Acc. 115, 361–369.

Carmen Berasain, M.J.P., Ujue Latasa, Maria, Castillo, Josefa, Goñi, Saioa, Santamaría, Mónica, Prieto, Jesús, Avila, Matías A., 2009. The epidermal growth factor receptor: a link between inflammation and liver cancer. Exp. Biol. Med. 234, 713–725.

Chaudhry, A.R., Ahmed, R., Irfan, A., Muhammad, S., Shaari, A., Al-Sehemi, A.G., 2014. Effect of heteroatoms substitution on electronic, photophysical and charge transfer properties of naphtha [2,1-b:6,5-b′] difuran analogues by density functional theory. Comp. Theor. Chem. 1045, 123–134.

Chen, X., Jia, C., Wan, Z., Zhang, J., Yao, X., 2014. Theoretical investigation of phenothiazine–triphenylamine-based organic dyes with different π spacers for dye-sensitized solar cells. Spectrochim. Acta A 123, 282–289.

Duflos, M., Nourrisson, M.-R., Brelet, J., Courant, J., LeBaut, G., Grimaud, N., Petit, J.-Y., 2001. N-Pyridinyl-indole-3-(alkyl)carboxamides and derivatives as potential systemic and topical inflammation inhibitors. Eur. J. Med. Chem. 36, 545–553.

Frisch, G.W.T.M.J., Schlegel, H.B., Scuseria, G.E., Robb, M.A., Cheeseman, J.R., Scalmani, G., Barone, V., Mennucci, B., Petersson, G.A., Nakatsuji, H., Caricato, M., Li, X., Hratchian, H.P., Izmaylov, A.F., Bloino, J., Zheng, G., Sonnenberg, J.L., Hada, M., Ehara, M., Toyota, K., Fukuda, R., Hasegawa, J., Ishida, M., Nakajima, T., Honda, Y., Kitao, O., Nakai, H., Vreven, T., Montgomery Jr., J.A., Peralta, J.E., Ogliaro, F., Bearpark, M., Heyd, J.J., Brothers, E., Kudin, K.N., Staroverov, V.N., Kobayashi, R., Normand, J., Raghavachari, K., Rendell, A., Burant, J.C., Iyengar, S.S., Tomasi, J., Cossi, M., Rega, N., Millam, J.M., Klene, M., Knox, J.E., Cross, J.B., Bakken, V., Adamo, C., Jaramillo, J., Gomperts, R., Stratmann, R.E., Yazyev, O., Austin, A.J., Cammi, R., Pomelli, C., Ochterski, J.W., Martin, R.L., Morokuma, K., Zakrzewski, V.G., Voth, G.A., Salvador, P., Dannenberg, J.J., Dapprich, S., Daniels, A.D., Farkas, Ö.,

Foresman, Ortiz, J.V., Cioslowski, J., Fox, D.J., 2009. Gaussian 09, Revision A. 01. Gaussian Inc, Wallingford, CT.

Fu, J.-J., Duan, Y.-A., Zhang, J.-Z., Guo, M.-S., Liao, Y., 2014. Theoretical investigation of novel phenothiazine-based D–π–A conjugated organic dyes as dye-sensitizer in dye-sensitized solar cells. Comp. Theor. Chem. 1045, 145–153.

Hamilton, L.M., Torres-Lozano, C., Puddicombe, S.M., Richter, A., Kimber, I., Dearman, R.J., Vrugt, B., Aalbers, R., Holgate, S.T., Djukanović, R., Wilson, S.J., Davies, D.E., 2003. The role of the epidermal growth factor receptor in sustaining neutrophil inflammation in severe asthma. Clin. Exp. Allergy 33, 233–240.

Irfan, A., 2014. First principle investigations to enhance the charge transfer properties by bridge elongation. J. Theor. Comput. Chem. 13, 1450013.

Irfan, A., 2014a. Modeling of efficient charge transfer materials of 4,6-di(thiophen-2-yl)pyrimidine derivatives: Quantum chemical investigations. Comp. Mater. Sci. 81, 488–492.

Irfan, A., 2014b. Highly efficient renewable energy materials benzo [2,3-b]thiophene derivatives: Electronic and charge transfer properties study. Optik – Intern. J. Light Elect. Optics 125, 4825–4830.

Irfan, A., Al-Sehemi, A.G., 2014. DFT study of the electronic and charge transfer properties of perfluoroarene–thiophene oligomers. J. Saudi. Chem. Soc. 18, 574–580.

Irfan, A., Al-Sehemi, A.G., Al-Assiri, M.S., 2014. Push–pull effect on the electronic, optical and charge transport properties of the benzo [2,3-b]thiophene derivatives as efficient multifunctional materials. Comp. Theor. Chem. 1031, 76–82.

Irfan, A., Al-Sehemi, A.G., Al-Assiri, M.S., 2014. The effect of donors–acceptors on the charge transfer properties and tuning of emitting color for thiophene, pyrimidine and oligoacene based compounds. J. Fluorine Chem. 157, 52–57.

Irfan, A., Al-Sehemi, A.G., Muhammad, S., Al-Assiri, M.S., Chaudhry, A.R., Kalam, A., Shkir, M., 2015. Electro-optical and charge injection investigations of the donor-π-acceptor triphenylamine, oligocene–thiophene–pyrimidine and cyanoacetic acid based multifunctional dyes. J. King Saud Univ. Sci. 27, 361–368.

Irfan, A., Muhammad, S., Al-Sehemi, A.G., Al-Assiri, M.S., Kalam, A., Chaudhry, A.R., 2015a. The effect of anchoring groups on the electro-optical and charge injection in triphenylamine derivatives@Ti6O12. J. Theor. Comput. Chem. 14, 1550027.

Irfan, A., Muhammad, S., Al-Sehemi, A.G., Al-Assiri, M.S., Kalam, A., 2015b. Structure modification to tune the electronic and charge transport properties of solar cell materials: quantum chemical study. Int. J. Electrochem. Sci 10, 3600–3612.

Irfan, A., Al-Sehemi, A.G., Muhammad, S., Chaudhry, A.R., Al-Assiri, M.S., Jin, R., Kalam, A., Shkir, M., Asiri, A.M., 2015c. In-depth quantum chemical investigation of electro-optical and charge-transport properties of trans-3-(3,4-dimethoxyphenyl)-2-(4-nitrophenyl)prop-2-enenitrile. C. R. Chim. 18, 1289–1296.

Irfan, A., Al-Sehemi, A.G., Rasool Chaudhry, A., Muhammad, S., 2016. The structural, electro-optical, charge transport and nonlinear optical properties of oxazole (4Z)-4-Benzylidene-2-(4-methylphenyl)-1,3-oxazol-5(4H)-one derivative. J. King Saud Univ. Sci. http://dx.doi.org/10.1016/j.jksus.2016.10.004.

Katrin Palm, K.L., Ungell, Anna-Lena, Strandlund, Gert, Beigi, Farideh, Lundahl, Per, Artursson, Per, 1998. Evaluation of dynamic polar molecular surface area as predictor of drug absorption: comparison with other computational and experimental predictors. J. Med. Chem. 41, 5382–5392.

Kelder, J., Grootenhuis, P.J., Bayada, D., Delbressine, L.C., Ploemen, J.-P., 1999. Polar molecular surface as a dominating determinant for oral absorption and brain penetration of drugs. Pharm. Res. 16, 1514–1519.

Kim, M.-S., Kim, J.-E., Lim, D.Y., Huang, Z., Chen, H., Langfald, A., Lubet, R.A., Grubbs, C.J., Dong, Z., Bode, A.M., 2014. Naproxen induces cell-cycle arrest and apoptosis in human urinary bladder cancer cell lines and chemically induced cancers by targeting PI3K. Cancer Prev. Res. 7, 236.

Kohn, W., Becke, A.D., Parr, R.G., 1996. Density functional theory of electronic structure. J. Phys. Chem. 100, 12974–12980.

Li, Y., Zou, L.-Y., Ren, A.-M., Feng, J.-K., 2012. Theoretical study on the electronic structures and photophysical properties of a series of dithienylbenzothiazole derivatives. Comp. Theor. Chem. 981, 14–24.

Lipinski, C.A., 2004. Lead- and drug-like compounds: the rule-of-five revolution. Drug Discovery Today: Technol. 1, 337–341.

Lipinski, C.A., Lombardo, F., Dominy, B.W., Feeney, P.J., 1997. Experimental and computational approaches to estimate solubility and permeability in drug discovery and development settings. Adv. Drug Deliv. Rev. 23, 3–25.

Lipinski, C.A., Lombardo, F., Dominy, B.W., Feeney, P.J., 2001. Experimental and computational approaches to estimate solubility and permeability in drug discovery and development settings1. Adv. Drug Deliv. Rev. 46, 3–26.

Lubet, R.A., Scheiman, J.M., Bode, A., White, J., Minasian, L., Juliana, M.M., Boring, D.L., Steele, V.E., Grubbs, C.J., 2015. Prevention of chemically induced urinary bladder cancers by naproxen: protocols to reduce gastric toxicity in humans do not alter preventive efficacy. Cancer Prev. Res. 8, 296.

Miehlich, B., Savin, A., Stoll, H., Preuss, H., 1989. Results obtained with the correlation energy density functionals of becke and Lee, Yang and Parr. Chem. Phys. Lett. 157, 200–206.

Musa, K.A.K., Eriksson, L.A., 2008. Theoretical study of the phototoxicity of naproxen and the active form of nabumetone. J. Phys. Chem. A 112, 10921–10930.

Nakka, M.S.B.M., Varaprasad, B.F.M., Reddy, L.V., Bhattacharya, A., Helliwell, M., Mukherjee, A.K., Beevi, S.S., Mangamoori, L. N., Mukkanti, K., Pal, S., 2010. Naproxen and ibuprofen based acyl hydrazone derivatives: synthesis, structure analysis and cytotoxicity studies. J. Chem. Pharm. Res. 2, 393–409.

Petersson, G.A., Al-Laham, M.A., 1991. A complete basis set model chemistry. II. Open-shell systems and the total energies of the first-row atoms. J. Chem. Phys. 94, 6081–6090.

Sadasivam, K., Jayaprakasam, R., Kumaresan, R., 2012. A DFT study on the role of different OH groups in the radical scavenging process. J. Theor. Comput. Chem. 11, 871–893.

Salvatori, P., Amat, A., Pastore, M., Vitillaro, G., Sudhakar, K., Giribabu, L., Soujanya, Y., De Angelis, F., 2014. Corrole dyes for dye-sensitized solar cells: The crucial role of the dye/semiconductor energy level alignment. Comp. Theor. Chem. 1030, 59–66.

Skehan, P., Storeng, R., Scudiero, D., Monks, A., McMahon, J., Vistica, D., Warren, J.T., Bokesch, H., Kenney, S., Boyd, M.R., 1990. New colorimetric cytotoxicity assay for anticancer-drug screening. J. Natl Cancer Inst. 82, 1107–1112.

Soteras Gutiérrez, I., Lin, F.-Y., Vanommeslaeghe, K., Lemkul, J.A., Armacost, K.A., Brooks Iii, C.L., MacKerell Jr., A.D., 2016. Parametrization of halogen bonds in the CHARMM general force field: improved treatment of ligand–protein interactions. Biorg. Med. Chem. 24, 4812–4825.

van de Waterbeemd, H., Camenisch, G., Folkers, G., Chretien, J.R., Raevsky, O.A., 1998. Estimation of blood-brain barrier crossing of drugs using molecular size and shape, and H-bonding descriptors. J. Drug Target. 6, 151–165.

Vanommeslaeghe, K., MacKerell Jr., A.D., 1850. CHARMM additive and polarizable force fields for biophysics and computer-aided drug design. Biochimica et Biophysica Acta (BBA) – Gen. Subj. 1850, 861–871.

Viale, M., Anzaldi, M., Aiello, C., Fenoglio, C., Albicini, F., Emionite, L., Gangemi, R., Balbi, A., 2013. Evaluation of the anti-proliferative activity of three new pyrazole compounds in sensitive and resistant tumor cell lines. Pharmacol. Rep. 65, 717–723.

Vichai, V., Kirtikara, K., 2006. Sulforhodamine B colorimetric assay for cytotoxicity screening. Nat. Protoc. 1, 1112–1116.

Wright, J.S., Johnson, E.R., DiLabio, G.A., 2001. Predicting the activity of phenolic antioxidants: theoretical method, analysis of

substituent effects, and application to major families of antioxidants. J. Am. Chem. Soc. 123, 1173–1183.

Youssef, A.M., Sydney White, M., Villanueva, E.B., El-Ashmawy, I. M., Klegeris, A., 2010. Synthesis and biological evaluation of novel pyrazolyl-2,4-thiazolidinediones as anti-inflammatory and neuroprotective agents. Biorg. Med. Chem. 18, 2019–2028.

Zgierski, M.Z., Lim, E.C., Fujiwara, T., 2014. Intramolecular charge transfer in di-tert-butylaminobenzonitriles and 2,4,6-tricyanoanilines: A computational TDDFT study. Comp. Theor. Chem. 1036, 1–6.